

Magnetic Excitations in the High T_c Iron Pnictides

D. X. Yao and E. W. Carlson

Department of Physics, Purdue University, West Lafayette, IN 47907

(Dated: November 4, 2018)

We calculate the expected finite frequency neutron scattering intensity based on the two-sublattice collinear antiferromagnet found by recent neutron scattering experiments as well as by theoretical analysis on the iron oxypnictide $LaOFeAs$. We consider two types of superexchange couplings between Fe atoms: nearest-neighbor coupling J_1 and next-nearest-neighbor coupling J_2 . We show how to distinguish experimentally between ferromagnetic and antiferromagnetic J_1 . Whereas magnetic excitations in the cuprates display a so-called resonance peak at (π, π) (corresponding to a saddlepoint in the magnetic spectrum) which is at a wavevector that is at least close to nesting Fermi-surface-like structures, no such corresponding excitations exist in the iron pnictides. Rather, we find saddlepoints near $(\pi, \pi/2)$ and $(0, \pi/2)$ (and symmetry related points), which are not close to nesting the Fermi surfaces.

PACS numbers: 74.25.Ha, 74.70.-b, 75.30.Ds, 76.50.+g

The recent discovery of superconductivity exceeding 50K in a new class of materials holds tremendous potential for understanding the origin of high temperature superconductivity. [1, 2, 3, 4, 5, 6] Similar to the cuprate superconductors, the iron pnictides also have a layered structure, and display magnetism in the undoped parent compound. Both become superconducting upon doping. And like the cuprates, the transition metal layer is believed to play an important role in the superconducting pairing. On the other hand, the parent compound of $LaOFeAs$ is a poor metal at room temperature, as opposed to a correlated insulator as in the cuprates.

Initially band structure calculations suggested the materials are nonmagnetic but close to a strong magnetic instability.[7, 8, 9] However, subsequent calculations have shown that the antiferromagnetic state has lower energy than the nonmagnetic state because of Fermi surface nesting.[10, 11, 12] In Ref. 12, a stripe-like antiferromagnetic ground state was suggested based on strong nesting effects. Recent neutron scattering experiments[13] have shown that the parent compound of $LaOFeAs$ is a long-range ordered antiferromagnet with a type of spin stripe order (*i.e.* unidirectional spin density wave). However the magnetic moment was found to be $0.36(5)\mu_B$ per iron, which is much smaller than the calculated value of $\sim 2.3\mu_B$ per iron. [10, 11, 12].

From an analysis of the superexchange interactions, Ref. 14 suggested that the next-nearest-neighbor interaction J_2 is antiferromagnetic (AFM), while the nearest-neighbor interaction J_1 is ferromagnetic (FM). However a first-principles band structure calculation predicts that the nearest-neighbor interaction is also antiferromagnetic.[15, 16] They predict that $|J_2|$ is almost as twice large as J_1 . In both cases, the competition between J_1 and J_2 leads to a type of stripe-ordered two-sublattice antiferromagnetic ground state (Fig 1) when $|J_2/J_1|$ is larger than the critical value.[17, 18] While the interactions J_1 and J_2 can compete, the uniaxial SDW

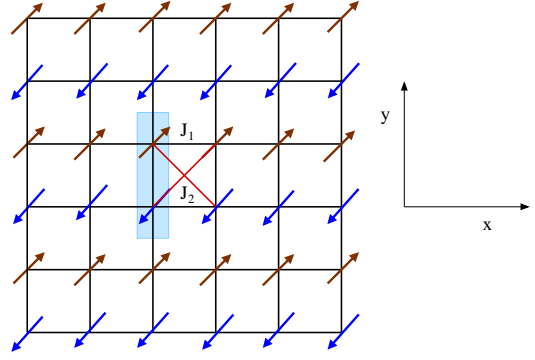


FIG. 1: (Color online) Two-sublattice collinear antiferromagnet on the Fe -square lattice. Shaded region is the magnetic unit cell.

considered in Fig. 1 is a classical ground state of the system, and it is thus not frustrated in the sense of having a macroscopic ground state degeneracy.

We use linearized spin wave theory to calculate the magnetic excitations and sublattice magnetization for the two-sublattice collinear antiferromagnet with nearest-neighbor superexchange coupling J_1 and antiferromagnetic next-nearest-neighbor superexchange coupling J_2 . We present results for ferromagnetic coupling J_1 as well as for antiferromagnetic coupling J_1 . (See Fig. 1.) We find the results are quite different for the two cases, so that comparing our calculations with future neutron scattering results at finite frequency will be able to distinguish these two cases.

The model Hamiltonian is described by the Heisenberg spin model on the square lattice

$$H = J_1 \sum_{\langle ij \rangle_{nn}} \mathbf{S}_i \cdot \mathbf{S}_j + J_2 \sum_{\langle ij \rangle_{nnn}} \mathbf{S}_i \cdot \mathbf{S}_j \quad (1)$$

where $\langle ij \rangle_{nn}$ and $\langle ij \rangle_{nnn}$ mean the nearest-neighbor and next-nearest-neighbor spin pairs respec-

tively. There are two spins in each unit cell, as shown in Fig. 1. We study the elementary excitations of the classical ground state of this model by using the well-known Holstein- Primakoff boson method. The dispersion and intensities are calculated by quantizing the classical spin waves.

We use Holstein-Primakoff bosons to quantize about the collinear antiferromagnetic ground state found in recent neutron scattering.[13]

$$H = E_{Cl} + S \sum_{\mathbf{k}} [A_{\mathbf{k}} a_{\mathbf{k}}^+ a_{\mathbf{k}} + \frac{1}{2} (B_{\mathbf{k}} a_{\mathbf{k}}^+ a_{-\mathbf{k}}^+ + B_{-\mathbf{k}}^* a_{\mathbf{k}} a_{-\mathbf{k}})] \quad (2)$$

where $E_{Cl} = -2J_2 N S^2$ is the classical ground state energy and

$$A_{\mathbf{k}} = (4J_2 + 2J_1 \cos k_x), \quad (3)$$

$$B_{\mathbf{k}} = (2J_1 \cos k_y + 4J_2 \cos k_x \cos k_y). \quad (4)$$

We can diagonalize the Hamiltonian using the Bogoliubov transformation

$$b_{\mathbf{k}} = \cosh \theta_{\mathbf{k}} a_{\mathbf{k}} - \sinh \theta_{\mathbf{k}} a_{-\mathbf{k}}^+. \quad (5)$$

The diagonalized Hamiltonian is

$$H = \sum_{\mathbf{k}} \omega(\mathbf{k}) b_{\mathbf{k}}^+ b_{\mathbf{k}} + E_{Cl} + E_0 \quad (6)$$

where $\omega(\mathbf{k})$ is the spin wave dispersion

$$\omega(\mathbf{k}) = S \sqrt{A_{\mathbf{k}}^2 - B_{\mathbf{k}}^2}, \quad (7)$$

and E_0 is the quantum zero-point energy correction

$$E_0 = \frac{S}{2} \sum_{\mathbf{k}} (-A_{\mathbf{k}} + \omega(\mathbf{k})). \quad (8)$$

For $|J_1| = 1$ and $J_2 = 2$, we get $E_0 = -0.332NS$.

We find that there is only one spin wave band

$$\omega(k_x, k_y) = \frac{2S \sqrt{(2J_2 + J_1 \cos k_x)^2 - (J_1 \cos k_y + 2J_2 \cos k_x \cos k_y)^2}}{2}. \quad (9)$$

The associated spin wave velocities are

$$v_x = 2S \sqrt{-J_1^2 + 4J_2^2}, \quad (10)$$

$$v_y = 2S |J_1 + 2J_2|. \quad (11)$$

Notice that v_x becomes imaginary for $|J_1| > 2|J_2|$, indicating a change in the classical ground state configuration.

Fig. 2 shows the spin wave band with the nearest neighbor coupling both antiferromagnetic (Fig. 2(a)) and ferromagnetic (Fig. 2(b)). The presence of saddlepoints can be seen, and we will return to this point later. In addition, because the (π, π) point is a magnetic reciprocal

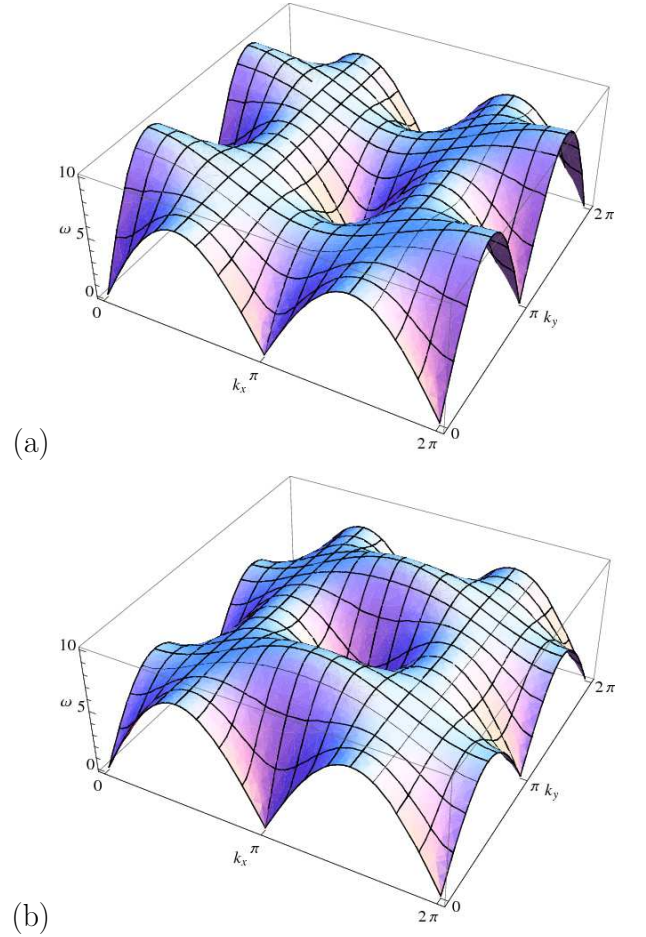


FIG. 2: (Color online) Spin-wave dispersion band for the two-sublattice collinear antiferromagnet shown in Fig. 1. (a) Dispersion with both couplings antiferromagnetic. Here we have set $J_1 = 1$ (AFM) with $J_2 = 2$ (AFM). (b) Dispersion with ferromagnetic nearest neighbor coupling. Here we have set $J_1 = -1$ (FM) with $J_2 = 2$ (AFM).

lattice vector, the dispersion must have $\omega \rightarrow 0$ at this point, although as we will see there is no zero-frequency intensity associated with this part of the dispersion. This precludes finite frequency weight at the (π, π) point from this band.

We calculate the zero-temperature dynamic structure factor using the same method, [19, 20]

$$S(\mathbf{k}, \omega) = \sum_f \sum_{i=x,y,z} |\langle f | S^i(\mathbf{k}) | 0 \rangle|^2 \delta(\omega - \omega_f). \quad (12)$$

Here $|0\rangle$ is the magnon vacuum state and $|f\rangle$ denotes the final state of the spin system with excitation energy ω_f . S^z does not change the number of magnons, contributing to the elastic part of the structure factor. $S^x(\mathbf{k})$ and $S^y(\mathbf{k})$ contribute to the inelastic dynamic structure factor through single magnon excitations.

In Figs. 3 and 4, we show the expected neutron scattering intensity for constant energy cuts in \mathbf{k} -space. We

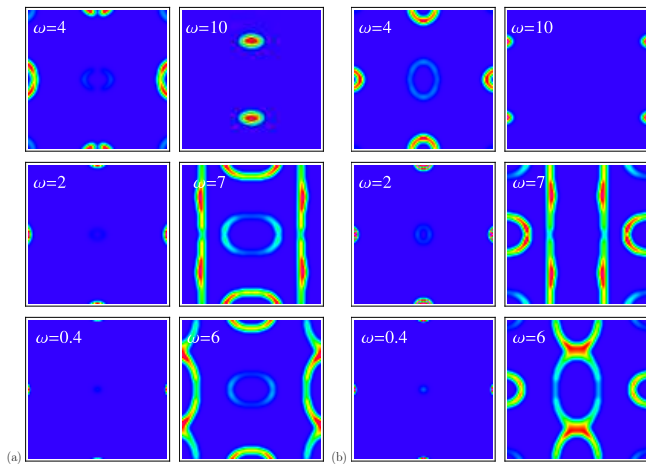


FIG. 3: (Color online) Constant-energy cuts (untwinned) of the dynamic structure factor $S(\mathbf{k}, \omega)$ for $J_2 = 2$ (AFM): (a) $J_1 = -1$ (FM), (b) $J_1 = 1$ (AFM). The x-axis and y-axis correspond to k_x and k_y respectively with the range $(0, 2\pi)$. We have integrated over an energy window of $\pm 0.2|J_1|S$.

show our predictions from spin wave theory for both ferromagnetic and antiferromagnetic J_1 . Fig. 3 shows the expected neutron scattering intensity from a single domain of the magnetic order (*i.e.* for an untwinned case), and Fig. 4 shows the expected scattering intensity for the case where there is an equal contribution from domains with both orientations of the magnetic order (*i.e.* for a twinned case).

For ferromagnetic J_1 , at low frequency, the strongest diffraction peaks are located at $(0, \pi)$. (See Fig. 3.) However more intensity weight shifts to $(\pi, 0)$ when J_1 is antiferromagnetic. There is also a spin wave cone emerging from (π, π) , but the intensity is much weaker than the cones emanating from other magnetic reciprocal lattice vectors, since zero frequency weight is forbidden at (π, π) for the magnetic order we consider. At high energy, the difference between ferromagnetic J_1 and antiferromagnetic J_1 becomes more apparent. For example, for FM J_1 , there are two strong spots along the (π, k_y) direction, whereas for AFM J_1 , they are along the $(0, k_y)$ direction. In real materials, stripe order can be twinned due to, *e.g.*, a finite correlation length, local disorder pinning, or crystal twinning. Therefore we show the twinned constant energy cut plots in Fig. 4 for both FM and AFM nearest neighbor coupling J_1 .

As can be seen from the dispersion in Fig. 2, there are saddlepoints in the spin wave excitation spectrum at various points in k -space. For the case of both couplings antiferromagnetic, these occur at $(\pi/2, 0)$ and $(\pi, \pi/2)$ and symmetry related points. For ferromagnetic nearest neighbor coupling, saddlepoints can be seen at $(0, \pi/2)$ along with weak saddlepoints possible at $(\pi/2, 0)$ and $(\pi/2, \pi)$ and symmetry related points. The integrated intensity is generally large at such saddlepoints. In the

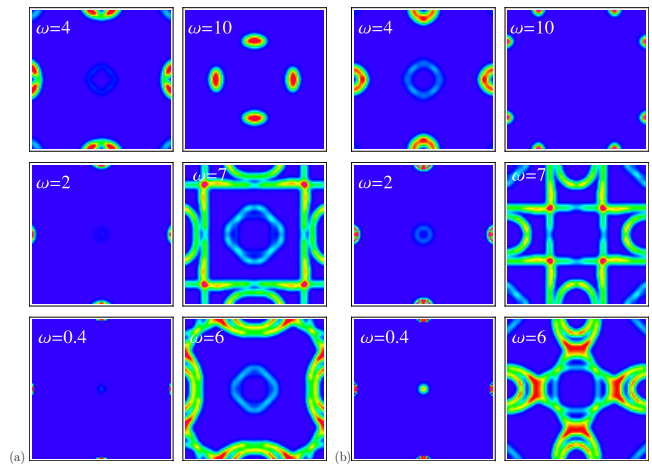


FIG. 4: (Color online) Constant-energy cuts (twinned) of the dynamic structure factor $S(\mathbf{k}, \omega)$ for $J_2 = 2$ (AFM): (a) $J_1 = -1$ (FM), (b) $J_1 = 1$ (AFM). The x-axis and y-axis correspond to k_x and k_y respectively with the range $(0, 2\pi)$. We have integrated over an energy window of $\pm 0.2|J_1|S$.

cuprates, there is a saddlepoint in the magnetic excitations at (π, π) which has been empirically connected to superconductivity, in that it increases in intensity at the onset of superconductivity, *i.e.* the “resonance peak”. There has been much discussion concerning this scattering phenomenon in the cuprates, particularly because it is close to nesting vectors for the corresponding Fermi surface. However, in the case of the iron pnictides, the saddlepoints we find here are quite far from any nesting vectors.

Experimentally, the magnetic moment per iron was found to be $0.36(5)\mu_B$, which is much smaller than the expected value of $\sim 2.3\mu_B$ per iron site.[10, 11, 12] The zero point energy of the spin waves reduces the sublattice magnetization. It was suggested in Ref. [14] that the competition between J_1 and J_2 may be responsible for the small moment observed in experiment. The sublattice magnetization m is defined as

$$m = \langle S_i^Z \rangle = S - \Delta m, \quad (13)$$

where Δm is the deviation of sublattice magnetization from the saturation value,

$$\begin{aligned} \Delta m &= \langle a_i^+ a_i \rangle \\ &= \sum_{\mathbf{k}} \langle a_{\mathbf{k}}^+ a_{\mathbf{k}} \rangle \\ &= \frac{1}{2V_{\mathbf{k}}} \sum_{\mathbf{k}} \left[\frac{SA_{\mathbf{k}}}{\omega(\mathbf{k})} - 1 \right] + \frac{1}{V_{\mathbf{k}}} \sum_{\mathbf{k}} \frac{SA_{\mathbf{k}}}{\omega(\mathbf{k})} \frac{1}{e^{\beta\omega(\mathbf{k})} - 1} \\ &= \Delta m^{quantum} + \Delta m^{thermal}. \end{aligned} \quad (14)$$

The first term $\Delta m^{quantum}$ comes from quantum zero point fluctuations. The second term $\Delta m^{thermal}$ comes from the classical thermal fluctuation, which is divergent

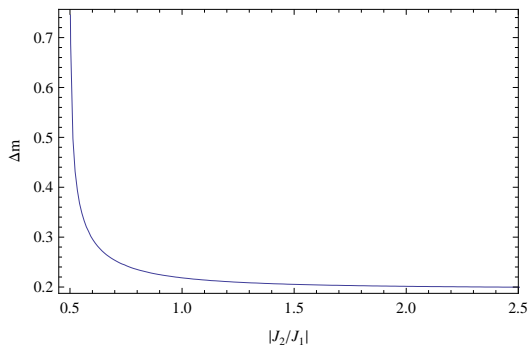


FIG. 5: $|J_2/J_1|$ dependence of the reduction of the sublattice magnetization due to zero point energy of the spin waves. Here we have used $|J_1| = 1$

at any finite temperature in agreement with the Mermin-Wagner theorem. (The very presence of the broken symmetry observed in experiment implies that there is some finite coupling between planes, however weak.)

Here we calculate $\Delta m^{quantum}$ by

$$\Delta m^{quantum} = \frac{1}{2} \int_0^{2\pi} \int_0^{2\pi} \frac{dk_x}{2\pi} \frac{dk_y}{2\pi} \frac{SA_{\mathbf{k}}}{\omega(\mathbf{k})} - \frac{1}{2}. \quad (15)$$

It is difficult to get the analytical form of the integral. Thus we numerically calculate $\Delta m^{quantum}$. From the symmetry, the above integral does not change when J_1 changes sign. In Fig. 5, $\Delta m^{quantum}$ is plotted as a function of the superexchange coupling ratio $|J_2/J_1|$. It is S -independent. If S is in between 1 and $\frac{3}{2}$, it will reduce the m by 13% – 20%. $\Delta m^{quantum}$ decreases with increasing J_2/J_1 because stonger J_2 stabilizes the two-sublattice collinear antiferromagnet state. This deviation is not sufficient to explain the observed value of the sublattice magnetization.

In conclusion, we have used spin wave theory to calculate the magnetic excitations and sublattice magnetization for the two-sublattice collinear antiferromagnetic state of the new $La(O_{1-x}F_x)FeAs$ high- T_c superconductors. We have studied both ferromagnetic and antiferromagnetic nearest-neighbor coupling J_1 with antiferromagnetic next-nearest-neighbor coupling J_2 . We calculate the predicted inelastic neutron scattering pattern based on spin wave theory. Comparison with future inelastic neutron scattering studies can be used to distinguish the sign of J_1 . We find that the sublattice magnetization can be reduced by the zero-point motion of spin waves, although not enough to account for the small moments observed in experiment. In addition, we iden-

tify several saddlepoints in the magnetic excitation spectrum. While magnetic excitations in these regions are expected to have extra intensity due to the saddlepoint structure, these corresponding wavevectors are not near nesting vectors of the Fermi surface.

We thank J. P. Hu, Y. L. Loh and A. Overhauser for helpful discussions. D. X. Y. acknowledges support from Purdue University. E. W. C is supported by Research Corporation.

Note added: Some results from spin wave calculations have also been reported by Ref. [21].

-
- [1] Y. Kamihara, T. Watanabe, M. Hirano, and H. Hosono, *J. Am. Chem. Soc.* p. 3296 (2008).
 - [2] L. Shan, X. Z. Y. Wang, G. Mu, L. Fang, and H.-H. Wen, arXiv:0803.2405 .
 - [3] H.-H. Wen, G. Mu, L. Fang, H. Yang, and X. Zhu, *Europhys. Lett.* **82**, 17009 (2008).
 - [4] X. H. Chen, T. Wu, G. Wu, R. H. Liu, H. Chen, and D. F. Fang, arXiv:0803.3603 .
 - [5] Z. A. Ren, J. Yang, W. Lu, W. Yi, G. C. Che, X. L. Dong, L. L. Sun, and Z. X. Zhao, arXiv:0803.4283 .
 - [6] Z. A. Ren, W. Lu, J. Yang, W. Yi, Z. C. L. X. L. Shen, G. C. Che, X. L. Dong, L. L. Sun, F. Zhou, and Z. X. Zhao, arXiv:0804.2053 .
 - [7] D. Singh and M. Du, arXiv:0803.0429 .
 - [8] K. Haule, J. H. Shim, and G. Kotliar, arXiv:0803.1279 .
 - [9] G. Xu, W. Ming, Y. Yao, X. Dai, S. Zhang, and Z. Fang, arXiv:0803.1282 .
 - [10] C. Cao, P. J. Hirschfeld, and H.-P. Cheng, arXiv:0803.3236 .
 - [11] F. Ma and Z.-Y. Lu, arXiv:0803.3286 .
 - [12] J. Dong, H. J. Zhang, G. Xu, Z. Li, G. Li, W. Z. Hu, D. Wu, G. F. Chen, X. Dai, J. L. Luo, Z. Fang, and N. L. Wang, arXiv:0803.3426 .
 - [13] C. de la Cruz, Q. Huang, J. W. Lynn, W. R. I. J. Li, J. L. Zarestky, H. A. Mook, G. F. Chen, J. L. Luo, N. L. Wang, and P. Dai, *Nature* **453**, 899 (2008).
 - [14] Q. Si and E. Abrahams, arXiv:0804.2480 .
 - [15] F. Ma, Z. Y. Lu, and T. Xiang, arXiv:0804.3370 .
 - [16] S. Ishibashi, K. Terakura, and H. Hosono, arXiv:0804.2963 .
 - [17] P. Chandra, P. Coleman, and A. I. Larkin, *Phys. Rev. Lett.* **64**, 88 (1990).
 - [18] N. Shannon, T. Momoi, and P. Sindzingre, *Phys. Rev. Lett.* **96**, 027213 (2006).
 - [19] E. W. Carlson, D. X. Yao, and D. K. Campbell, *Phys. Rev. B* **70**, 064505 (2004).
 - [20] D. X. Yao, E. W. Carlson, and D. K. Campbell, *Phys. Rev. Lett.* **97**, 017003 (2006).
 - [21] C. Fang, H. Yao, W.-F. Tsai, J. P. Hu, and S. A. Kivelson, arXiv:0804.3843 .